Acta Acustica united with Acustica
Vol. 104 (2018) 396 – 409

DOI 10.3813/AAA.919183

Perfect Absorption of Sound by Rigidly-Backed High-Porous Materials

Noé Jiménez, Vicent Romero-García, Jean-Philippe Groby
Laboratoire d'Acoustique de l'Université du Maine (LAUM) - CNRS UMR 6613,
Av. Olivier Messiaen, 72085 Le Mans, France. noe.jimenez@univ-lemans.fr

Summary

We present the conditions to observe perfect sound absorption by rigidly-backed layers of rigid-frame high-porous materials. We theoretically analyze different configurations of increasing complexity: a single layer of high-porous material, a layer of high-porous material with an air gap (air plenum), and an optimized multilayer structure. First, we show that to obtain normal incidence perfect sound absorption at the first so-called quarter-wavelength resonance of a single rigidly-backed high-porous layer, the thickness of the material is strongly related to its flow resistivity. In particular, perfect sound absorption is observed when the quarter-wavelength resonance is around the characteristic Biot frequency of the high-porous media. We found that the optimal thickness of the layer is 4.64 smaller than the perfectly absorbed wavelength when using one-parameter empirical models for the effective parameters of the high-porous material. Then, we analyze the behavior of the structure for oblique angles of incidence, showing that perfect sound absorption is also produced for other incident angles and frequencies. Second, an air gap is introduced between the high-porous layer and the rigid backing. The gap allows to produce perfect sound absorption for structures thicker than the optimal one and for media with large intrinsic losses, i.e., for materials with high flow resistivity. Finally, optimized multilayer structures are proposed, which present broadband and perfect sound absorption. The existence of perfect absorption is related to the impedance matching, which is produced when the intrinsic losses of the system exactly compensate the leakage of the structure due to its resonance. Thus, to observe perfect sound absorption, in addition to and material properties, the total thickness of any multilayered porous structure is constrained to its quarter-wavelength resonance because of the lack of deep-subwavelength resonance in the system.

PACS no. 43.20.Gp, 43.20.Jr

1. Introduction

Traditionally, porous and fibrous materials have been the most widely used sound-absorbing materials due to their excellent absorption performance in a broad range of audible frequencies, their relative low manufacturing cost and low weight [1, 2]. These materials are composed of an elastic frame, which will be considered motionless in the present article, saturated by a host fluid, typically air. The micro-structure of porous media presents a representative scale much smaller than the characteristic wavelength of sound in air, the pore scale being of the order of the viscous and thermal boundary layers [1]. These materials allow sound waves to propagate through the structure with a slightly reduced sound speed than in air mainly due to the tortuosity and the strong attenuation because of thermal and viscous losses. The complex processes that experience the acoustic waves at the micro-scale in porous materials can be described at the macro-scale, in a good approximation, considering the porous media as a homogeneous fluid with effective complex and frequency dependent properties.

To observe acoustic absorption, the material/structure must be geometrically bounded. Two main configurations are commonly used. The first configuration allows sound transmission. A typical structure consists in placing the porous material layer between two elastic layers, e.g., plywood panels. This solution is commonly used to design "sandwich" panels for soundproofing in order to reduce as much as possible the acoustic transmission. In the second configuration, a layer of porous material is rigidly attached to an impervious wall, thus, no transmission is considered. This solution is commonly used in room acoustics to produce anechoic surfaces or to reduce noise levels in a given enclosure [1, 2]. In this paper, we will focus on the second configuration for the sake of simplicity, i.e., on a purely reflection problem. However, similar analysis can be conducted to transmission problems [3].

For a rigidly-backed porous material of total thickness L with a complex and frequency dependent effec-

Received 21 September 2017,
accepted 26 March 2018.

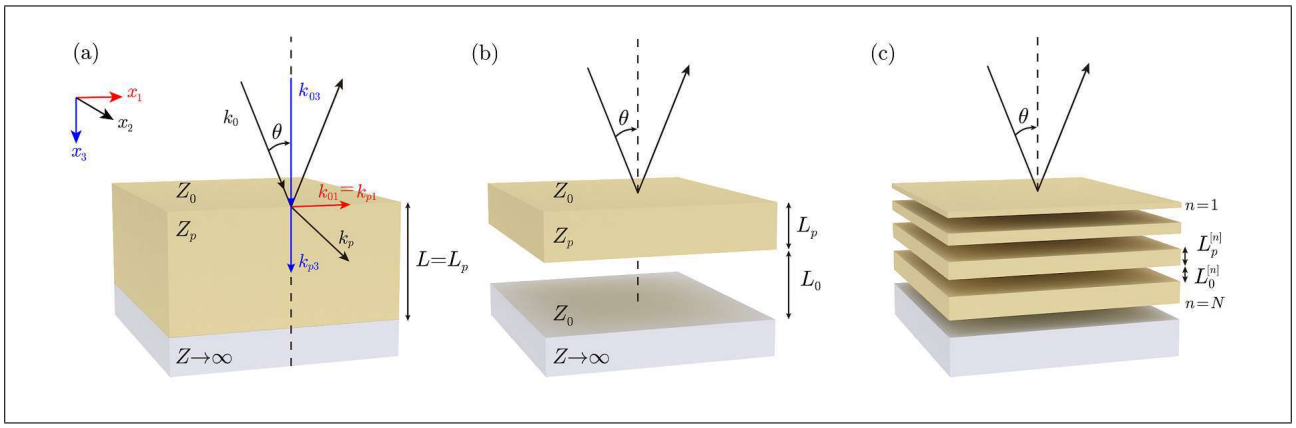

Figure 1. Scheme of the configurations, (a) rigidly-backed porous layer of length L_p, (b) Porous layer separated a distance L_0 from a rigid wall. (c) Multilayer structure composed of N alternating porous and air layers, where the n-th layers of air and porous material are of length $L_0^{[n]}$ and $L_p^{[n]}$ respectively.

tive wavenumber and characteristic impedance, k_e and Z_e respectively, the absorption coefficient, α, at normal incidence is given by

$$\alpha = 1 - \left| \frac{\mathrm{i} Z_e \cot k_e L - Z_0}{\mathrm{i} Z_e \cot k_e L + Z_0} \right|^2, \qquad (1)$$

where Z_0 is the impedance of the surrounding fluid, typically air. Thus, the absorption coefficient becomes unitary, i.e., perfect, when the acoustic impedance of the rigidly backed material, $\mathrm{i} Z_e \cot k_e L$, equals the impedance of the surrounding medium, i.e., when the material is impedance matched. Perfect acoustic absorption has been theoretically, numerically and experimentally observed in structures including subwavelength resonators, namely metamaterials. These perfectly absorbing metamaterials comprise propagation in waveguides [4, 5, 6], metaporous materials [7] and panels composed of quarter-wavelength resonators [8], Helmholtz resonators [9, 10, 11] or membrane and plate resonators [12, 13, 14].

For a rigidly-backed layer of porous material, the impedance matching condition can only be achieved for frequencies around $k_p L \approx n\pi/2$ with $n = 1, 3, \ldots$, i.e., at the so-called quarter-wavelength resonances (QWR) of the rigidly-backed material. Please note here, that the so-called quarter-wavelength resonances correspond to a vanishing numerator rather than to a vanishing denominator of the reflection coefficient. Therefore, they are interference phenomena and not resonant ones. Thus, the thickness of the porous layer must be large to obtain absorption at low frequencies and this could limit their use in practical applications. Note the typical wavelength of low frequency sound in air is of the order of several meters.

As a corollary, perfect absorption can only be reached at the first quarter-wavelength resonance when this resonance lies in the inertial regime and not in the viscous one. In the inertial regime, the imaginary part of the effective wavenumber inside the porous material, i.e., the attenuation, is strongly increased with respect to that of the air, while, in contrast, the real part of the wavenumber inside the material is almost similar to that of the air. In addition, the characteristic impedance in the porous material is also of the same order as that of the air. In the viscous regime, the pressure field satisfies a diffusion equation and the effective wavenumber inside the porous material is mostly imaginary, i.e. the attenuation is very large. We will focus on the relation between the condition for perfect absorption and the viscous/inertial transition, i.e., the Biot frequency of the porous material, rather than to the adiabatic/isothermal one.

In this work, we will analyze the conditions to obtain *perfect sound absorption* using layers of porous materials, i.e., the conditions under the absorption coefficient became exactly one at a particular frequency. To model the problem, we will make use of a standard theoretical approach based on transfer matrix method. We extend the analysis to oblique incidence, a porous material with a rigidly- backed air cavity and, finally, optimized multilayer structures.

2. Theoretical model

2.1. Description of the system

We consider layered structures of total thickness L, composed of N alternating layers of porous material and air, as shown in Figures 1a-c. The n-th layer is therefore composed of a $L_p^{[n]}$-thick porous layer and a $L_0^{[n]}$-thick air layer. For the sake of simplicity, each material is considered as a homogeneous and isotropic fluid.

The porous material is characterized by its complex and frequency dependent wavenumber, k_p, and characteristic impedance, Z_p, while the air is considered lossless characterized by its wavenumber, k_0, and characteristic impedance, Z_0, that are given by

$$\begin{aligned} k_0 &= \omega/c_0 = \omega\sqrt{\rho_0/\kappa_0}, \quad Z_0 = \sqrt{\rho_0\kappa_0}, \\ k_p &= \omega/c_p = \omega\sqrt{\rho_p/\kappa_p}, \quad Z_p = \sqrt{\rho_p\kappa_p}, \end{aligned} \qquad (2)$$

where c_p and c_0 are the effective sound speed in the porous material and in air respectively, ω is the angular frequency,

ρ_0, ρ_p and κ_0 and κ_p are the effective density and bulk modulus of the air and porous material, respectively.

We characterize the porous media by using various models. First, we consider the widely used empirical model proposed by Delany and Bazley (DB) [15], which only depends on the flow resistivity of the porous material, σ. This model was derived by fitting a frequency power-law to the measured acoustic response of various porous materials with porosity close to one, and is valid in the range $0.01 < \rho_0 f/\sigma < 1$. Despite the fact that it does not describe accurately the behavior of every porous material, it nevertheless provides reasonable values for the effective parameters for a wide range of porous and fibrous materials and frequencies with only one input parameter. Using the DB empirical model, the complex and frequency dependent wavenumber and characteristic impedance are given by

$$Z_p^{\mathrm{DB}} = Z_0 \left[1 + a_1\left(\frac{\rho_0 f}{\sigma}\right)^{b_1} - \mathrm{i}a_2\left(\frac{\rho_0 f}{\sigma}\right)^{b_2}\right],$$
$$k_p^{\mathrm{DB}} = k_0 \left[1 + a_3\left(\frac{\rho_0 f}{\sigma}\right)^{b_3} - \mathrm{i}a_4\left(\frac{\rho_0 f}{\sigma}\right)^{b_4}\right], \quad (3)$$

where the coefficients are $a_1 = 0.057$, $b_1 = -0.754$, $a_2 = 0.087$, $b_2 = -0.732$, $a_3 = 0.0978$, $b_3 = -0.700$, $a_4 = 0.189$, $b_4 = -0.595$.

A further refinement of the DB model was carried on by Miki [16]. This model used same data as the DB model, but the fitted coefficients corrects the non-physical result of the effective parameters of the original DB in the low frequency regime [16]. The expressions for the DBM model are

$$Z_p^{\mathrm{DBM}} = Z_0 \left[1 + a_1\left(\frac{f}{\sigma}\right)^{b_1} - \mathrm{i}a_2\left(\frac{f}{\sigma}\right)^{b_2}\right],$$
$$k_p^{\mathrm{DBM}} = k_0 \left[1 + a_3\left(\frac{f}{\sigma}\right)^{b_3} - \mathrm{i}a_4\left(\frac{f}{\sigma}\right)^{b_4}\right], \quad (4)$$

with the coefficients $a_1 = 0.07$, $a_2 = -0.107$, $a_3 = 0.109$, $a_4 = -0.16$, $b_1 = -0.632$, $b_2 = -0.632$, $b_3 = -0.618$, $b_4 = -0.618$. The limit of validity of this model is given by $0.01 < f/\sigma < 1$.

The third model we consider is the semi-phenomenological one proposed by Johnson-Champoux-Allard (JCA) [17, 18] that provides the expressions of the dynamic effective densities and bulk modulus of a porous material saturated by a fluid of density ρ_0 and bulk modulus κ_0. The porous material is characterized by 5 parameters, namely the porosity ϕ, the tortuosity α_∞, the flow resistivity σ, and the viscous and thermal characteristic lengths Λ and Λ' respectively. Thus, the expressions of the dynamic effective density and bulk modulus provided by the JCA model are

$$\rho_p^{\mathrm{JCA}} = \frac{\alpha_\infty \rho_0}{\phi}\left[1 - \mathrm{i}G_1(\omega)\sqrt{1 + \mathrm{i}G_2(\omega)}\right],$$

$$\kappa_p^{\mathrm{JCA}} = \frac{\gamma P_0/\phi}{\gamma - (\gamma-1)\left[1 - \mathrm{i}G_1'(\omega)\sqrt{1 + \mathrm{i}G_2'(\omega)}\right]^{-1}}, \quad (5)$$

where the functions $G_1(\omega)$, $G_2(\omega)$, $G_1'(\omega)$, $G_2'(\omega)$ are given by

$$G_1(\omega) = \frac{\sigma\phi}{\alpha_\infty \rho_0 \omega}, \qquad G_2(\omega) = \frac{4\alpha_\infty^2 \rho_0 \eta \omega}{\sigma^2 \phi^2 \Lambda^2},$$
$$G_1'(\omega) = \frac{8\eta}{\rho_0 \mathrm{Pr} \Lambda'^2 \omega}, \qquad G_2'(\omega) = \frac{\rho_0 \mathrm{Pr} \Lambda'^2 \omega}{16\eta}. \quad (6)$$

This model was further be extended by Lafarge [19] to accurately describe thermal effects in the low frequency regime. The extended model, namely the Johnson-Champoux-Allard-Lafarge (JCAL) model, uses a modified version of the effective bulk modulus and involves a new parameter, the static thermal permeability, k_0'. Using the JCAL model, the thermal effects are accounted by the modified functions $G_1'(\omega)$ and $G_2'(\omega)$, given by

$$G_1'(\omega) = \frac{\phi\eta}{\rho_0 \mathrm{Pr} k_0' \omega}, \qquad G_2'(\omega) = \frac{4\rho_0 \mathrm{Pr} k_0'^2 \omega}{\eta \Lambda'^2 \phi^2}, \quad (7)$$

while the viscous effects are accounted in the same manner than in the JCA model, i.e., $G_1(\omega)$ and $G_2(\omega)$ remains the same.

We consider that the surrounding and saturating fluid is air, $\rho_0 = 1.213\,\mathrm{kg/m^3}$, $\mathrm{Pr} = 0.71$ is the Prandtl number, $\gamma = 1.4$ is the ratio of the specific heats, $P_0 = 101325\,\mathrm{Pa}$ is the atmospheric pressure, $\eta = 1.839\ 10^{-5}\,\mathrm{kg\,m^{-1}s^{-1}}$ is the dynamic viscosity, and the sound speed in air is given by $c_0 = \sqrt{\gamma P_0/\rho_0}$.

In this work, three configurations are studied, as shown in Figure 1. First, the conditions for perfect absorption of a simple rigidly-backed layer of porous material of thickness L_p are studied, as shown in Figure 1a. Second, the study is extended by introducing an air cavity of length L_0 between the porous material and the rigid backing, as shown in Figure 1b. Finally, the conditions for perfect absorption of a structure of $N = 4$ alternating layers of porous materials are analyzed, as shown in Figure 1c.

2.2. Transfer Matrix Method

The layered system is theoretically analyzed by using a general framework based on the transfer matrix method (TMM) [20]. We consider a plane wave impinging the structure with an incidence angle θ defined with respect to the outward normal to the structure, see Figure 1. Due to continuity of the wavevector along the interfaces, the wavenumber in the tangential direction x_1 is the same in all media, leading to

$$k_{01} = k_0 \sin(\theta), \quad k_{03} = \sqrt{k_0^2 - k_0^2 \sin^2(\theta)},$$
$$k_{p1} = k_0 \sin(\theta), \quad k_{p3} = \sqrt{k_p^2 - k_p^2 \sin^2(\theta)}, \quad (8)$$

where k_{01} and k_{p1} are the tangential (along x_1) components, and k_{03} and k_{p3} are the normal component (along

x_3) of the wavenumbers in the air and in the porous layer respectively, as shown in Figure 1a. Note that, due to symmetry considerations it is sufficient to consider only two components (k_3 and k_1) to describe the problem: in the case of a oblique incidence with a component in the direction x_2, a simple rotation of the reference system can be applied to reduce the transversal wavenumber to one component.

The Fourier Transform of the pressure, p, and normal particle velocity, v_3, at the boundaries $x_3 = 0$ and $x_3 = L$ are related by a transfer matrix $\mathbf{T}$ as

$$\begin{bmatrix} p \\ v_3 \end{bmatrix}_{x_3=0} = \mathbf{T} \begin{bmatrix} p \\ v_3 \end{bmatrix}_{x_3=L}. \tag{9}$$

This total transfer matrix $\mathbf{T}$ can be obtained by the product of the transfer matrices of each layer as

$$\mathbf{T} = \begin{bmatrix} T_{11} & T_{12} \\ T_{21} & T_{22} \end{bmatrix} = \prod_{n=1}^{N} \mathbf{T}^{[n]}, \tag{10}$$

where $\mathbf{T}^{[n]}$ is the transfer matrix of the n-th layer. In addition, the transfer matrix of the n-th layer, which is formed by two sublayers (air and porous material), can be defined as

$$\mathbf{T}^{[n]} = \begin{bmatrix} T_{11}^{[n]} & T_{12}^{[n]} \\ T_{21}^{[n]} & T_{22}^{[n]} \end{bmatrix} = \mathbf{T}_p^{[n]} \mathbf{T}_0^{[n]}, \tag{11}$$

where the transfer matrix of the n-th porous sublayer, $\mathbf{T}_p^{[n]}$, under oblique incidence is given by

$$\mathbf{T}_p^{[n]} = \begin{bmatrix} \cos k_{p3}^{[n]} L_p^{[n]} & \dfrac{\mathrm{i} Z_p^{[n]} k_p^{[n]}}{k_{p3}^{[n]}} \sin k_{p3}^{[n]} L_p^{[n]} \\ \dfrac{\mathrm{i} k_{p3}^{[n]}}{Z_p k_p^{[n]}} \sin k_{p3}^{[n]} L_p^{[n]} & \cos k_{p3}^{[n]} L_p^{[n]} \end{bmatrix}, \tag{12}$$

and the transfer matrix of the n-th air sublayer, $\mathbf{T}_0^{[n]}$, is written as

$$\mathbf{T}_0^{[n]} = \begin{bmatrix} \cos k_{03} L_0^{[n]} & \dfrac{\mathrm{i} Z_0 k_0}{k_{03}} \sin k_{03} L_0^{[n]} \\ \dfrac{\mathrm{i} k_{03}}{Z_0 k_0} \sin k_{03} L_0^{[n]} & \cos k_{03} L_0^{[n]} \end{bmatrix}. \tag{13}$$

Finally, the reflection coefficient of the rigidly-backed structure under oblique incidence is obtained by setting $v_3|_{x_3=L} = 0$. After some algebra, it can be written as a function of the elements of the total transfer matrix given in Equation (10) as

$$R = \frac{T_{11}\cos(\theta) - Z_0 T_{21}}{T_{11}\cos(\theta) + Z_0 T_{21}}. \tag{14}$$

Then, the absorption is calculated as usual as

$$\alpha = 1 - \left| R \right|^2. \tag{15}$$

In addition, the impedance at the first interface can be calculated from the reflection coefficient as

$$Z_s = \frac{Z_0}{\cos(\theta)} \frac{(1+R)}{(1-R)}. \tag{16}$$

The impedance at the first interface is useful to study the impedance matching of the structure with the exterior medium and to obtain the perfect absorption conditions. In general, perfect absorption is observed in a lossy open system when a structure is critically coupled with the exterior medium, i.e., when the intrinsic losses compensate the energy leakage of the resonating system [4]. This occurs when all the eigenvalues of the scattering matrix of the system are zero. In the particular case of a rigidly-backed structure, the scattering matrix is only represented by the reflection coefficient and, therefore, perfect absorption is observed when all reflected waves vanish. Analyzing Equation (16), the condition for perfect absorption can be directly identified. It reduces to the well-known impedance matching condition $Z_s \cos(\theta) = Z_0$. Assuming a lossless exterior medium, $\mathrm{Im}(Z_0) = 0$, and Z_s being generally complex, perfect absorption only can be observed when

$$\frac{\mathrm{Re}\,(Z_s)}{Z_0}\cos\theta = 1 \quad \text{and} \quad \mathrm{Im}\,(Z_s) = 0, \tag{17}$$

which are the well-known impedance matching conditions. In the following sections, we will analyze specific rigidly-backed configurations in order to derive the conditions for perfect sound absorption using porous media.

3. Rigidly-backed porous layer

We start the analysis by considering a simple layer of porous material of thickness $L = L_p$, as shown in Figure 1a. In the case of a rigidly-backed layer, the generalized TMM leads to a simple expression of the reflection coefficient, which is recalled here for the sake of completeness. After some algebra, the acoustic impedance given by Equation (16) reduces to

$$Z_s = -\mathrm{i} Z_p \frac{k_p}{k_{p3}} \cot k_{p3} L, \tag{18}$$

while the reflection coefficient is written as

$$R = \frac{Z_s \cos(\theta) - Z_0}{Z_s \cos(\theta) + Z_0}. \tag{19}$$

To obtain perfect absorption, the impedance matching conditions given by Equation (17) must be fulfilled, leading to $\mathrm{Im}(-\mathrm{i} Z_p k_p / k_{p3} \cot k_{p3} L) = 0$. This is fulfilled when $k_{p3} L = n\pi/2$ with $n = 1, 3, 5, \ldots$, i.e, the perfect absorption can only be observed at the so-called quarter-wavelength resonances of the rigidly-backed medium. Note also the quarter-wavelength resonances depend on k_{p3}, then, the frequencies at which perfect absorption is observed depend on the incidence angle. Moreover, perfect absorption is achieved when $\mathrm{Re}(-\mathrm{i} Z_p k_p / k_{p3} \cot k_{p3} L)\cos(\theta) = Z_0$. Assuming that the characteristic impedance of the porous material is of the same order as that of the air, we find that to obtain perfect absorption $\mathrm{Re}(Z_p) \approx Z_0$ at normal incidence. However, note this is only an approximation because Z_p and

k_p are complex and frequency dependent. Thus, the different models of porous media will lead to slightly different conditions for perfect sound absorption.

3.1. Normal incidence

We start by calculating the absorption of a rigidly-backed porous layer of varying thickness, using the DBM model. Without loss of generality, we normalize the porous thickness by the wavelength $\lambda_0 = c_0/f_0$ at the Biot frequency of the porous material given by

$$f_0 = \frac{\sigma\phi}{2\pi\alpha_\infty\rho_0}. \tag{20}$$

This important parameter indicates the transition between the inertial and the viscous regime of the porous material, and only depends on the material parameters. It is worth noting here that, although Biot's theory is not used in this paper, this simple ratio can be used to characterize the material, as we will see in the following sections.

For the present study, we start fixing $f_0 = 1000$ Hz, and setting $\phi = 1$ and $\alpha_\infty = 1$ for the sake of simplicity. Thus, the Biot frequency becomes linearly dependent on the flow resistivity, that for this example is $\sigma = 2\pi f_0\alpha_\infty\rho_0/\phi = 7.6$ kRayls/m. Figure 2a shows the absorption of the layer for different thicknesses: $L = \lambda_0/2, \lambda_0/4, \lambda_0/4.64$ and $\lambda_0/8$, using the DBM model. On the one hand, the first quarter-wavelength resonance for the thinnest layer ($L = \lambda_0/8$) appears around 2 kHz. However, we can see that even at the resonance frequency of the rigidly-backed layer the absorption is far from unity. On the other hand, the first quarter-wavelength resonance of the thickest layer ($L = \lambda_0/2$) appears around 500 Hz. In the same way, the absorption is also far from perfect. For the chosen porous material parameters, the absorption is near unity around 800 Hz, at $L \approx \lambda_0/4$. However, because Z_p and k_p are complex and frequency dependent, the quarter-wavelength resonance appears at $L = \lambda_0/4.64$. To accurately determine the resonance frequency of the porous layer, Figure 2 (b) shows the reflection coefficient in logarithmic scale, as a function of the frequency and for the different thicknesses considered. Here, the lowest frequency dip, marked with the dashed circle, corresponds to the maximum absorption produced at the quarter-wavelength resonance, appearing at $L = \lambda_0/4.64$ and $f = 1000$ Hz.

To derive the conditions that provide perfect absorption, it is useful to analyze the system in the complex frequency plane. Thus, Figures 3a-c show the reflection coefficient in the complex frequency plane $f = f_r + \mathrm{i}f_i$ for the previous layer thicknesses. In this configuration, the zeros of the reflection coefficient are associated to the so-called quarter-wavelength resonances. Please note that despite the fact that the so-called quarter-wavelength resonances are not resonant phenomena (because they correspond to vanishing numerator of R), they are strongly linked to the real mode of the rigidly-backed porous layer, corresponding to vanishing denominators of R. Effectively, in the absence of losses, both zeros and poles are complex conjugate in the complex frequency plane.

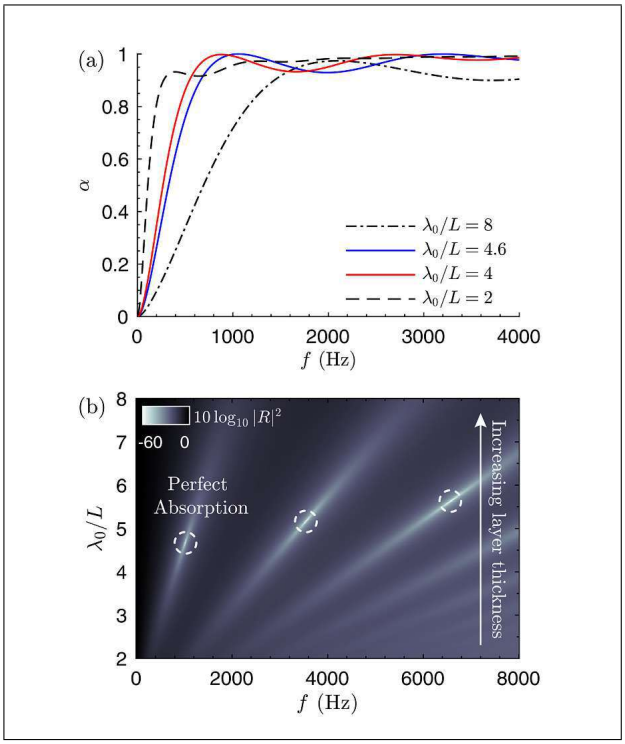

Figure 2. (a) Absorption produced by a layer of rigidly-backed porous material of various thickness. (b) Map of the reflection coefficient as a function of the layer thickness normalized to the Biot characteristic wavelength ($\lambda_0 = 2\pi c_0\rho/\sigma$). Color map in logarithmic scale, $10\log_{10}|R|^2$.

First, Figure 3a shows the case of a thin layer of thickness $L = \lambda_0/8$. We can see that the first quarter-wavelength resonance appears at $f_r = 2000$ Hz. However, the effect on the absorption of this zero is moderate, because it is located far from the real frequency axis ($f_i = 800$ Hz) in the upper half-space. This means that the amount of losses of the system is not sufficient to exactly compensate the leakage Note that to achieve perfect absorption a zero of the reflection coefficient must be exactly located at the real frequency axis.

The position of the zeros of the reflection coefficient can be drawn as a function of the layer thickness L, their positions in the complex plane being marked by the blueish lines in Figure 3. By increasing the thickness of the porous layer, the resonance is shifted to lower frequencies and the zero approaches the real frequency axis. The movement to lower imaginary frequencies is related to the increase of the amount of total losses of the rigidly-backed system. Thus, we can see that for $L = \lambda_0/4.64$, as shown in Figure 3b, the lowest frequency zero is exactly located at the real frequency axis. For this set of parameters, the impedance matching conditions are fulfilled and perfect absorption is observed: the intrinsic losses of the porous material exactly compensate the energy leakage of the quarter-wavelength resonant system.

Then, when the layer thickness is increased to $L = \lambda_0/4$, the lowest frequency zero crosses the real frequency axis towards the half-plane where the poles of the system

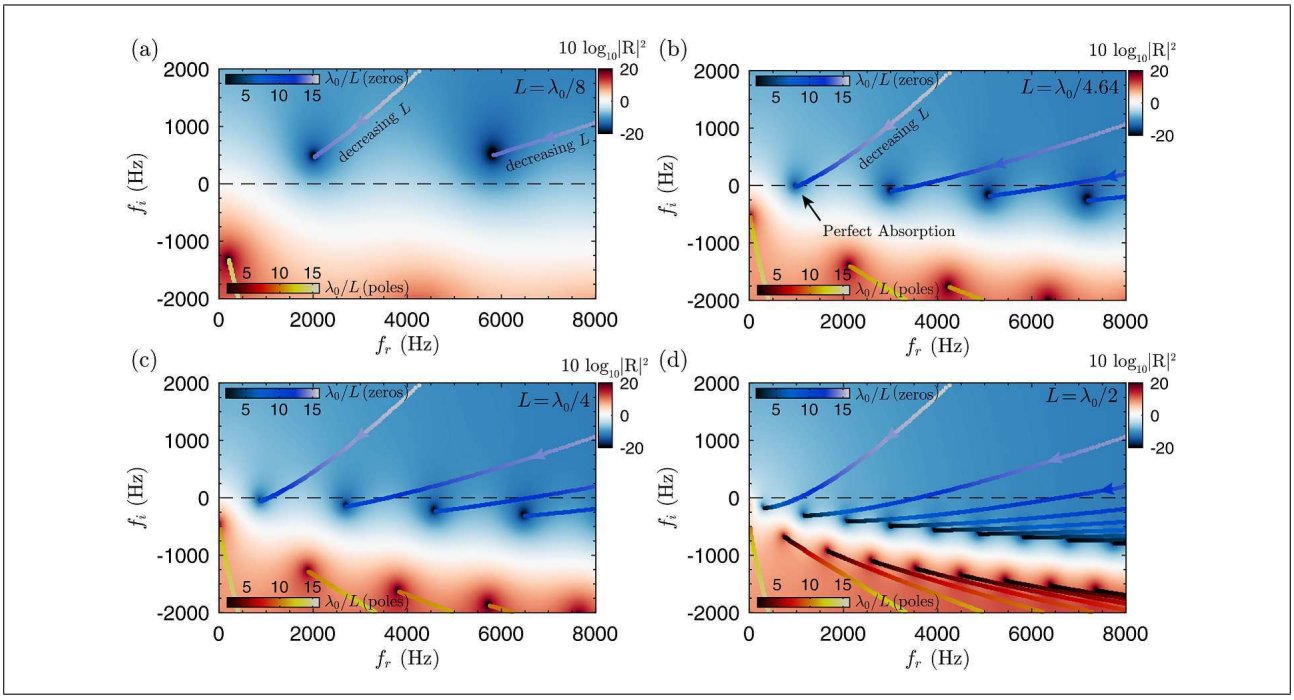

Figure 3. (Colour online) Complex frequency representation of the reflection coefficient in logarithmic scale. The trajectories of the zeros (blueish) and poles (reddish) lines are marked as a function of the panel thickness. (a) $L = \lambda_0/8$, (b) Critically coupled configuration, $L = \lambda_0/4.64$, (c) $L = \lambda_0/4$ and (d) $L = \lambda_0/2$.

are located. Some energy is reflected back due to a non-perfect impedance matching, because the intrinsic losses of the system are too large. Therefore, the absorption is large but not perfect, because the zero still located close to the real frequency axis.

Finally, if the layer thickness is again increased, as shown in Figure 3d, the resonance frequency of the rigidly-backed layer appears at frequencies much lower than the Biot frequency. Then, the diffusive processes dominate the propagation inside the porous material and a strong reflection is produced by the rigidly-backed material. It is worth noting here that the Biot frequency depends only on the material parameters. Then, for a given material, with fixed flow resistivity, perfect absorption at the first quarter-wavelength resonance can be only achieved at a unique value of the material thickness and at a single frequency.

3.2. The conditions for perfect absorption

The exact conditions to observe perfect absorption in rigidly-backed porous layers depend on the model considered for the effective parameters of the porous material. Here, we obtain the conditions for perfect absorption as a function of the flow resistivity and layer thickness by using optimization methods. Thus, the cost function for the optimization process is directly $\epsilon = |R|^2$, and we look for the flow resistivity value and layer thickness that impedance match the structure to the surrounding medium. We initially set $\alpha_\infty = 1$, $\phi = 1$, for the DB, DBM, JCA and JCAL models, setting $\Lambda = 40$ μm, $\Lambda' = 2\Lambda$ for JCA and JCAL models, and $\kappa_0' = 1\ 10^{-8}$ m^2 for JCAL. The result of this optimization is shown in Figures 4a-b.

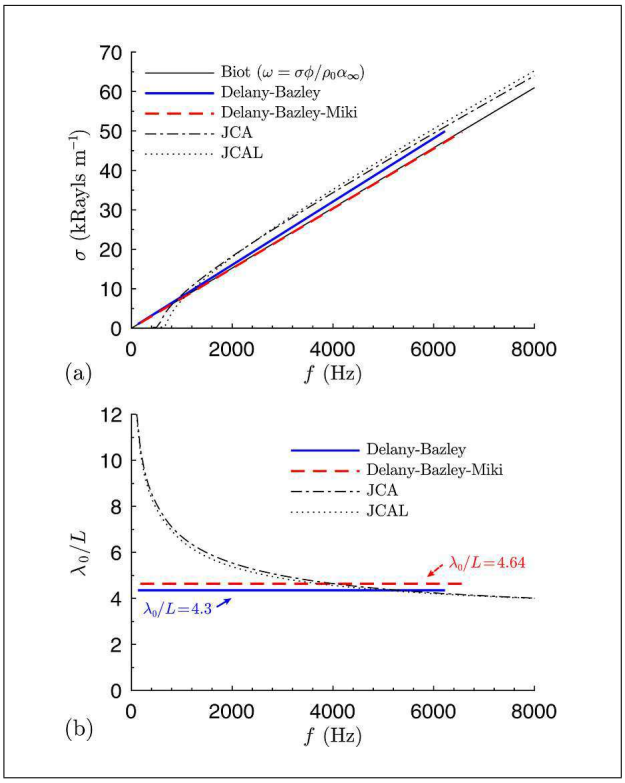

Figure 4. Critical coupling conditions for a layer of porous material. (a) Flow resistivity as a function of the frequency at which perfect absorption is observed, calculated using different models. (b) Layer thickness condition for perfect absorption, normalized to the Biot characteristic wavelength ($\lambda_0 = 2\pi c_0\rho/\sigma$).

On the one hand, the required flow resistivity to observe a peak of perfect absorption at a given frequency

is shown in Figure 4a. the Biot frequency is marked in black line as a reference. First, we can see that the Biot frequency, although not exact, is a very accurate estimation for the critical coupling conditions, specially using DB or DBM models. However, the specific conditions depend on the model used to estimate the effective parameters k_p and Z_p. Using either DB or DBM models, a linear dependence is observed between the flow resistivity and the impedance matched frequency. For high and medium frequency sound waves, both JCA and JCAL give similar linear dependences. However, discrepancies between JCA and JCAL are observed below 1000 Hz, caused by the differences in the modeling of the thermal effects provided by both JCA and JCAL models. Note that if the input material parameters are properly estimated, the JCAL will give the most accurate characterization of the effective parameters.

On the other hand, the required layer thickness to observe perfect absorption at a given frequency is shown in Figure 4b. For the DBM model, the quarter-wavelength resonance producing perfect absorption is observed at $\lambda_0/L \approxeq 4.64$. Thus, for a given porous material, perfect absorption only can be observed if the thickness of the layer is 4.64 times smaller than the Biot characteristic wavelength of the material. DB model presents a very small difference, being the ratio $\lambda_0/L \approxeq 4.3$. These values are independent of frequency. However, this is not the case when using more accurate models like JCA or JCAL. Using these models the layer thickness shows a more complex dependence on the critically coupling frequency, and the ratio λ_0/L becomes bigger for lower frequencies, as shown in Figure 4b. It is worth noting that the ratio is bigger than $\lambda_0/L > 4$ for audible sound frequencies below 6 kHz. This implies that even for low tortuosity materials, $\alpha_\infty = 1$, the quarter wavelength resonance is shifted-down to low frequencies.

This analysis can be extended to study the effect of porosity and tortuosity. In Figure 5 we show the critical coupling conditions using JCA and JCAL models using different porosities and tortuosities.

On the one hand, Figure 5a shows the required flow resistivity to produce perfect absorption at a given frequency, for various porosities. The reference Biot frequency is marked in dotted lines. We can observe that for materials with low tortuosity and high porosity (black lines), the required flow resistivity to produce perfect absorption is similar to the given by the Biot frequency. This implies that for a given material with low tortuosity and high porosity, the perfectly absorbed frequency can be estimated by $\omega \approx \sigma\phi/\rho_0\alpha_\infty$. This behavior is maintained for materials with relatively low porosities and low tortuosity (blue line in Figure 5a), although differences can be observed, specially for low frequencies. Only small differences are observed using JCA (continuous lines) or JCAL (dashed lines) models. The corresponding normalized thickness required to observe the perfect absorption is shown in Figure 5b. We note that, using both models, when the porosity is increased keeping the tortuosity constant, only a small effect on the layer thickness required

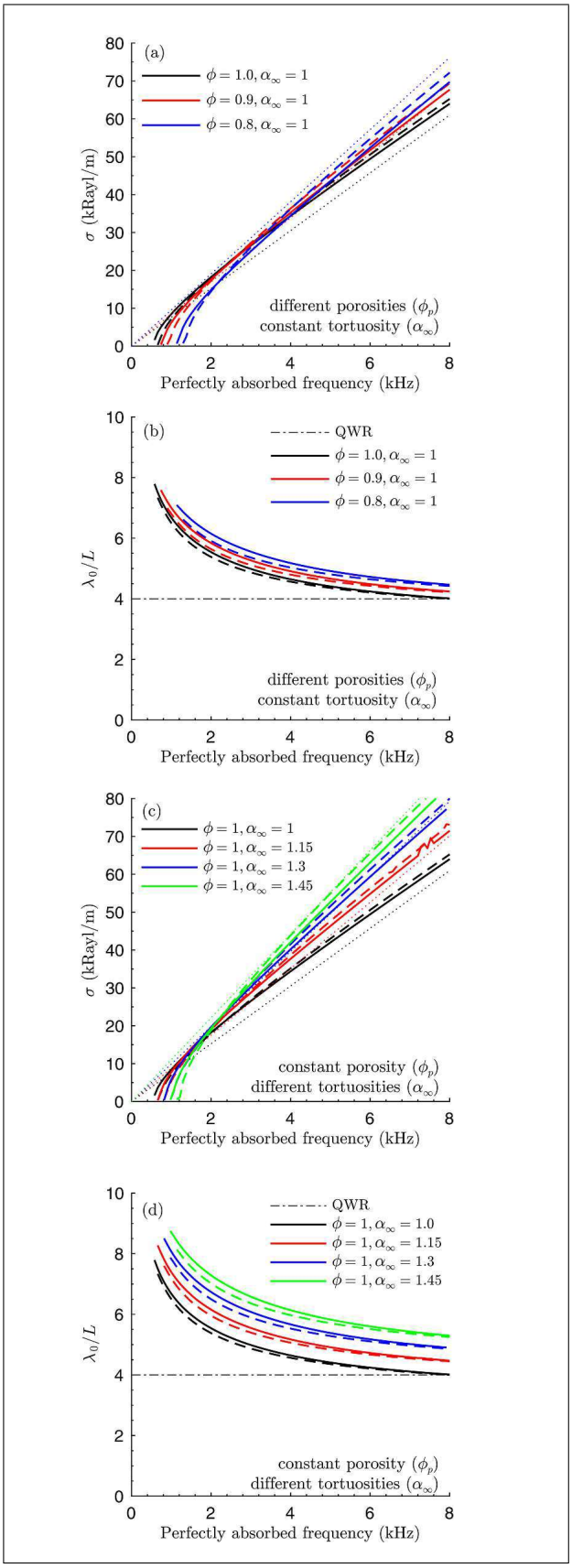

Figure 5. (Colour online) Critical coupling conditions using JCA model (continuous) and JCAL (dashed) using different porosities and tortuosities. The reference of Biot frequency is marked in dotted lines in (a,c), while the quarter wavelength resonance is marked in (b,d) with a black dashed line.

to produce perfect sound absorption is observed: samples with lower porosity require less thickness.

On the other hand, Figure 5c shows the required flow resistivity to produce perfect absorption at a given frequency, for various values of tortuosity. For materials with high porosity and low tortuosity (black and red lines in Figure 5c), we observe that the required flow resistivity to produce perfect absorption is similar to the given by the Biot frequency. However, for materials with high tortuosity and high porosity, the flow resistivity only follow the simple expression $\sigma = f\rho_0\alpha_\infty/2\pi\phi$ to produce perfect absorption at a frequency f at high frequencies. Using this expression the flow resistivity is overestimated at low frequencies. In addition, we observe in Figure5d that for high porosity and high tortuosity materials, the layer thickness can be strongly reduced below the quarter wavelength resonance, i.e., $\lambda_0/L > 4$. This is caused by the well-known tortuosity effect, that increases the total path traveled by the sound in the material. Then, the effective sound speed in the material is reduced respect to that of the air, down-shifting the quarter wavelength resonance frequency of the porous layer. This effect is stronger in the low frequency regime. However, note that for these frequencies the required flow resistivity is very low. In this way, it will be difficult to design materials with a microstructure that presents simultaneously high tortuosity, high porosity and low flow resistivity.

3.3. Oblique incidence

In the following, we will present the performance of the critically coupled porous media under oblique incidence, using the DBM model. The impedance of an isotropic porous media does not depend on the angle of incidence. The behavior of locally reacting media under oblique incidence has been described previously, e.g. in [10, 21]. In particular, in [21] metamaterials composed of narrow ducts were analyzed. The main difference between locally reacting materials and layers of porous material is that the term k_{p3} depends on the incident angle for the porous media. Therefore, the trajectories of the zeros and poles along the complex frequency plane in porous media present another degree of freedom compared to those presented for locally reacting metamaterials in [21].

Figure 6 shows the trajectories of the zeros and poles of the reflection coefficient of porous layers as a function of the incidence angle, varying the angle from $\theta = 0°$ (normal) to $\theta = 90°$ (grazing). We show the trajectories for the four different porous thicknesses previously analyzed. First, Figure 6a shows the trajectories of the zeros and poles for a thin layer of thickness $L = \lambda_0/8$. Note the value at $\theta = 0$ corresponds to Figure 3a, i.e., for the case that the layer is not critically coupled for normal incidence. However, the zeros and poles move in the complex plane for oblique incidence angles because both, the axial component of the wavenumber in the porous layer given by Equation (8) and the reflection coefficient given by Equations (18), (19) are functions of the angle of incidence. Eventually, the trajectories of the zeros along the complex frequency plane could cross the real axis, as can be observed for $\theta = 55.7°$. At this specific angle, the reflection coefficient vanishes, as shown in Figure 6b, and perfect sound absorption is achieved at $f = 5013$ Hz. Note that, following the trajectories, the zero that produces the perfect absorption at oblique incidence is not the one at lowest frequency, i.e., the perfect absorption for this configuration is produced by the second QWR.

In the same way, Figures 6c,d show the case of a layer of porous material of optimal thickness using the DBM model, $L = \lambda_0/4.64$. As previously seen, the absorption is perfect at $f = 1000$ Hz for normal incidence, i.e, a zero is located exactly at the real frequency axis for normal incidence, as shown in Figure 6c. Therefore, a peak of perfect absorption is produced, as marked by the red circle in Figure 6d. However, for oblique incidence the reflection coefficient changes and the location of the zero is shifted in the complex frequency plane towards higher frequencies. We can see that its trajectory in the complex plane follows an arc, eventually crossing again the real frequency axis at $f_r = 2105$ Hz for $\theta = 51.2$ °. Thus, a new peak of perfect sound absorption is produced, as marked by the corresponding red circle in Figure 6d.

We have shown that for $L = \lambda_0/4.64$ the structure was critically coupled for the first quarter-wavelength resonance at normal incidence. However, as shown in the complex plane Figure 6c, the second and higher resonances can also produce peaks of perfect absorption when their corresponding zeros cross the real frequency axis. This occurs for the second resonance at $\theta = 33.7$ ° and $f_r = 3770$ Hz, and $\theta = 44.5$ ° and $f_r = 4730$ Hz (blue circles in Figure 6d); and for the third resonance at $\theta = 40.64$ ° and $f_r = 7120$ Hz.

For a layer which is thicker than the optimal value at normal incidence, the zeros of the reflection coefficient appears in the same complex frequency half-plane than its corresponding poles. In this case, two situations can occur. If the layer is near the optimal, as shown in Figure 6e,f for $L = \lambda/4$, some of the trajectories of the zeros can cross the real frequency axis for oblique angles of incidence. Thus, some peaks of perfect absorption can be obtained in the same way as previously explained. When the layer is too thick compared with the optimal for normal incidence the starting point is far from the real frequency axis, as shown in Figure 6g,h for $L = \lambda/2$. The trajectories of the zeros of the reflection coefficient for such a thick layer never cross the real frequency axis. Therefore, no impedance matching can be produced even for oblique angles of incidence. This is explained physically because this frequency lies in the viscous regime of the porous material and the pressure field satisfies a diffusion equation rather than a wave equation with small losses. Thus, no perfect absorption can be observed for any resonance because the losses of the system exceeds the leakage of energy due to the QWR resonance, as shown in Figure 6f.

Finally, we notice that to tilt the angle of incidence does not correspond to increase the porous layer thickness. This is particularly visible from Equations (18)–(19) and when

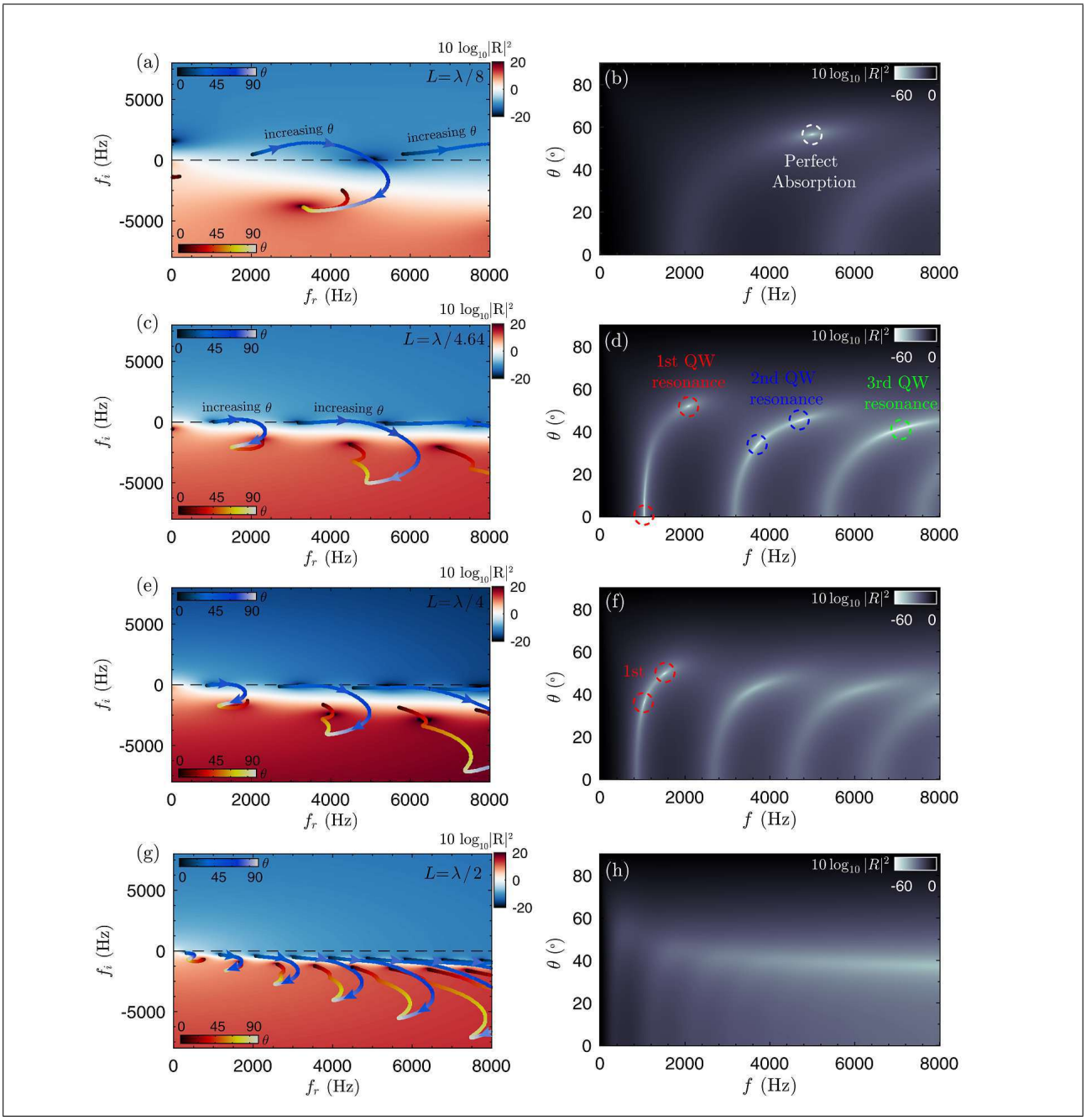

Figure 6. (Colour online) (a) Complex frequency representation of the reflection coefficient in logarithmic scale. The trajectories of the zeros (blueish) and poles (reddish) lines are traced as a function of incidence angle, θ, as indicated in the colorbars. (a) Layer thickness $L = \lambda_0/8$, (b) Reflection coefficient in logarithmic scale as a function of the incident angle. (c,d) Critically coupled configuration, $L = \lambda_0/4.64$, (e,f) $L = \lambda_0/4$. (g,h) $L = \lambda_0/2$.

comparing the zero trajectories reported in Figure 3c when the thickness increases and in Figure 6c, when the incident angle increases.

4. Porous layer with an air cavity

In the following, we introduce an air gap between the porous layer and the rigid-backing, as shown in Figure1b. It is well-known that in some cases using this configuration the low frequency regime of the absorption coefficient can be improved saving porous material [1], therefore it is widely used in practical applications [22]. Here, we focus on the conditions for obtaining perfect absorption for a porous layer at normal incidence with an air cavity using the DB model. In analogy with Equation (18), the impedance of the rigid-backed air gap is

$$Z_{\text{gap}} = -\mathrm{i}Z_0 \frac{k_0}{k_{03}} \cot k_{03} L_0, \tag{21}$$

where L_0 is the thickness of the air gap. Then, the impedance of the porous layer with the rigidly-backed cavity

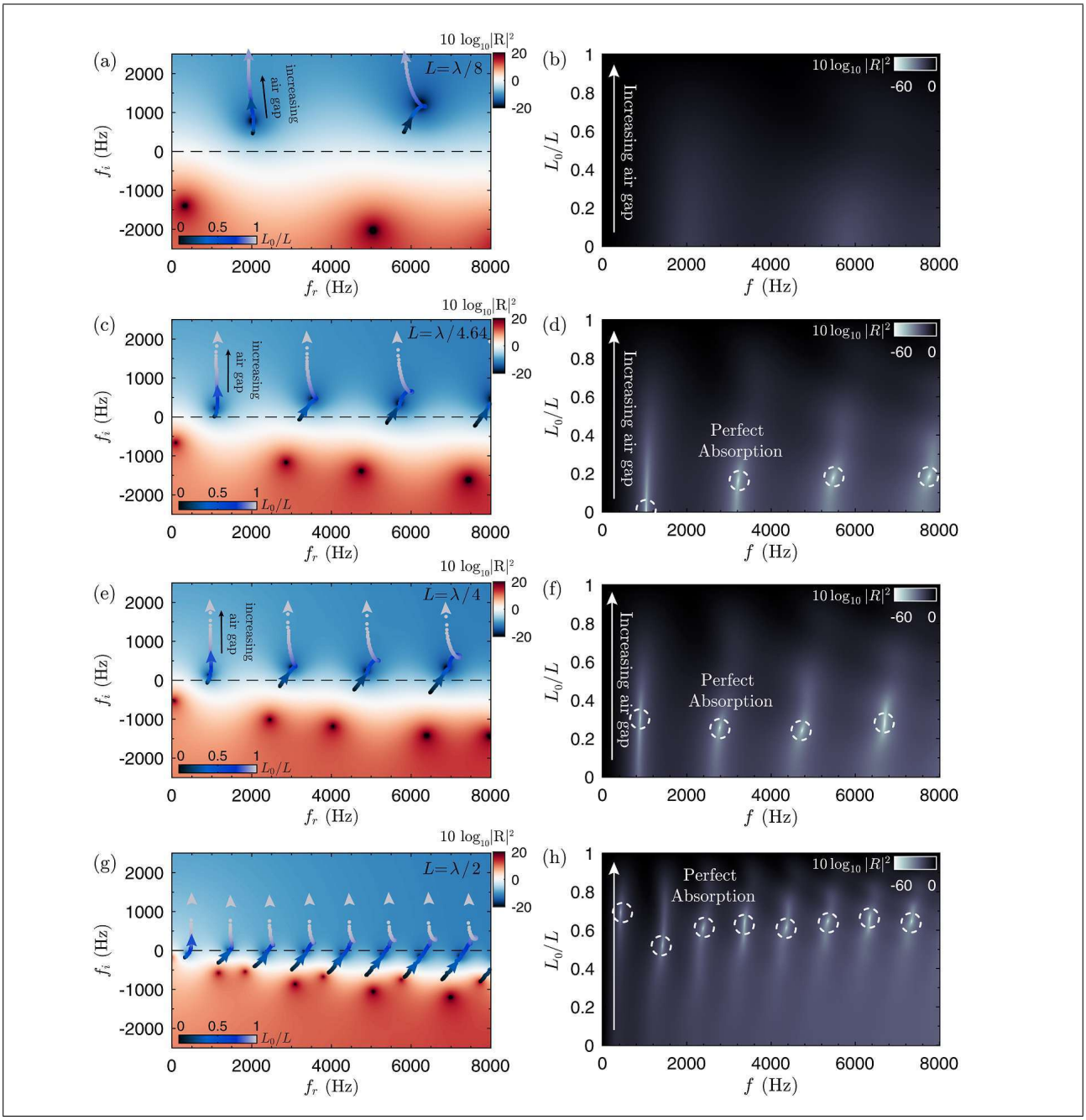

Figure 7. (Colour online) (a) Complex frequency representation of the reflection coefficient in logarithmic scale. The trajectories of the zeros (blueish) lines are traced as a function of the ratio of air gap and total thickness, L_0/L, being the total thickness constant, as indicated in the colorbars. (a) Layer thickness $L = \lambda_0/8$, (b) Reflection coefficient in logarithmic scale as a function of the incident angle. (c,d) Critically coupled configuration for normal incidence, $L = \lambda_0/4.64$, (e,f) $L = \lambda_0/4$. (g,h) $L = \lambda_0/2$.

reads as

$$Z_s = Z_p \frac{k_p}{k_{p3}} \left(\frac{-\mathrm{i} Z_{\mathrm{gap}} \cot\left(k_{p3} L_p\right) + Z_p k_p / k_{p3}}{Z_{\mathrm{gap}} - \mathrm{i} Z_p k_p / k_{p3} \cot\left(k_{p3} L_p\right)} \right). \quad (22)$$

The reflection coefficient and the absorption are calculated as usual using Equation (19).

We start using the results of the previous configurations. First, we define the total thickness of the layer as $L = L_p + L_0$, where L_p is the thickness of the porous material and L_0 is the thickness of the air gap. Thus, we will maintain constant the total thickness of the configuration, L, while the ratio between the porous layer and the air gap, L_0/L, will be modified from $L_0/L = 0$ (no gap) to $L_0/L \to 1$ (infinitesimal porous layer). It is worth noting here that for very thin layers of porous material the present model is not accurate: in a real situation, elastic modes will be produced in the poro-elastic plate. Here, for the sake of simplicity, we just consider the acoustic mode in the fluid like media.

Figure 7a,b shows the results for the case of a thin configuration of $L = \lambda_0/4$, where the quarter-wavelength resonance frequency is higher than the Biot frequency. In

Figure 7a we show the trajectories of the zeros of the reflection coefficient in the complex plane as the ratio between layers increases. We omit the poles for the sake of simplicity. We can see that when the air gap thickness increases the zeros move away from the real frequency axis in the upper half-space. The losses of the system are decreased. This can be explained because the effective impedance of the slab presents less intrinsic losses when the air gap increases. The leakage of the structure at its quarter-wavelength resonance around $f_r = 2000$ Hz cannot be compensated by the small intrinsic losses of this configuration [4]. Thus, at normal incidence no perfect absorption can be observed for a this thin layer of porous material, even when an air gap is introduced, as shown in Figure 7b.

The second case corresponds to the configuration using an optimal layer, i.e. $L = \lambda_0/4.64$. The results are shown in Figure 7c,d. As seen previously, perfect absorption is observed at $f = 1000$ Hz for the first quarter-wavelength resonance. However, at the frequencies of the higher resonances the absorption was not perfect: at these frequencies the losses were too large and the structure was not critically coupled. By increasing the air gap, we can decrease the losses of the system, then, eventually the leakage produced by the higher resonances can be exactly compensated and perfect absorption can be achieved. This situation corresponds to the crossing of the zeros of the real frequency axis in Figure 7c, and to the ratios of air/porous material marked by the circles in Figure 7d.

Analogous behavior is observed for layers thicker than the optimal at normal incidence, as shown in Figure 7e,f for $L = \lambda_0/4$ and Figure 7g,h for $L = \lambda_0/2$. In all these configurations the intrinsic losses of the rigidly-backed porous layer are too large compared to the leakage produced at their quarter-wavelength resonances, producing strong reflection. However, by introducing the air gap the losses of the slab of effective material can be reduced. Then, by tuning the ratio between the thickness of the porous layer and the thickness of the air gap, we can find the critical coupling conditions that produce perfect absorption for any resonance. It is worth noting here that the counterpart is that the absorption curve presents strong ripples in frequency.

5. Multilayer porous structures

Finally, we present perfect absorption for multi-layered structures with optimized parameters. The structures are composed of N alternating porous material and air layers, as shown in Figure1c. These structures were presented recently by some of the authors of the present work to demonstrate perfect absorption in a transmission problem [23], where the scattering matrix presents two different eigenvalues. Here, we present broadband perfect absorption for the rigidly-backed problem, where the scattering matrix only presents a single eigenvalue: the reflection coefficient.

We used optimization techniques to determine the total thickness and the flow resistivity of a total of $N = 4$ layers that maximize the absorption in the frequency range [500, 8000] Hz. We used the DBM model. The constraints were the total thickness of the structure, L, and the flow resistivity, that was bounded to $1 < \sigma < 50$ kRayls/m. We consider two cases, one of total length $L = 5$ cm and a second with $L = 10$ cm.

Table I. Geometrical parameters of the optimized multilayer structure of total thickness $L = 5$ cm.

	$n = 1$	$n = 2$	$n = 3$	$n = 4$
$L_p^{[n]}$ (cm)	1.66	1.53	1.81	0
$L_0^{[n]}$ (cm)	0	0	0	0
σ (kRayls/m)	3.13	13.00	50.00	-

Figure 8a,b shows the results for the first case ($L = 5$ cm) using the optimized layered structure, whose data is shown in Table I. The absorption curve is shown in Figure 8a. It shows a flat absorption curve where quasi-perfect absorption is observed over the optimized frequency range. However, despite its flatness, the absorption can only be perfect at the resonances of the structure. This can be observed in more detail in Figure8b, where the reflection coefficient is represented in the complex frequency plane. Perfect absorption is only produced when the reflection coefficient vanishes, and this only occurs at the zeros (blueish deeps) of the reflection coefficient. Each zero/pole pair is linked to a resonance of the rigidly-backed problem. We can also observe that the zero that appears at the lowest real frequency corresponds to the first quarter-wavelength resonance (around 2105 Hz). Below this frequency no resonance exists, therefore, the absorption curve decreases. It is worth noting here that as the sound speed in the porous material is similar to that in air, the rigidly-baked porous layer cannot be of deep-subwavelength thickness, even when the multilayer structure is optimized to maximize the impedance matching using a progressively increasing flow resistivity parameter. We show in Figure 8a a reference curve, which corresponds to a single layer with the same thickness, and with the optimal porosity given by $\sigma_{op} = 2\pi\rho_0 c_0/4.64L$ (see Section 3). In the case of $L = 5$ cm, $\sigma_{op} = 12.1$ kRayls/m. The reference layer produces a peak of perfect absorption at $f = 1558$ Hz, lower than the first resonance of the optimized multilayer. However, strong ripples are observed in comparison with the optimized multi-layered structure.

For the second case, we use a thicker layer, of total thickness $L = 10$ cm, leading to an optimal flow resistivity of $\sigma_{op} = 6.1$ kRayls/m (used in the reference curve). The quarter-wavelength resonance of the multilayer structure is down-shifted to $f = 977$ Hz in this case, while the reference layer gives a peak of perfect absorption at 795 Hz. The optimized geometry is shown in Table II.

The absorption curve of the optimized multilayer structure is shown in Figure 8c, showing an extremely flat absorption coefficient for frequencies above the quarter-wavelength resonance. Figure 8d shows the corresponding complex frequency plane. We can see that some of the

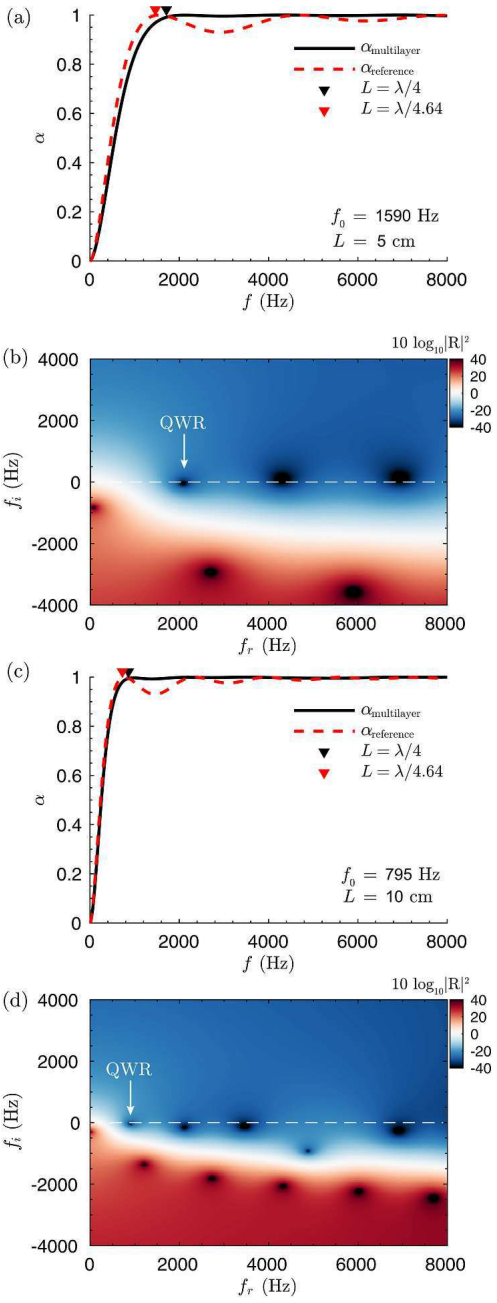

Figure 8. (Colour online) (a) Absorption for a optimized multilayer structure of $L = 5$ cm (black) and a reference homogeneous layer (dashed red) with optimal flow resistivity $\sigma_{Biot} = 2\pi\rho_0 c_0/4.644L$. The triangles mark the quarter-wavelength resonance ($f = c_0/4L$) and the optimal frequency ($f = c_0/4.64L$). (b) Corresponding representation of the reflection coefficient in the complex frequency plane. (c) Absorption for a optimized multilayer structure of $L = 10$ cm (black) and a reference homogeneous layer (dashed red). (d) Corresponding representation of the reflection coefficient in the complex frequency plane.

zeros of the refection coefficient are located on the real frequency axis, then, producing perfect absorption. The others, while not exactly in the real frequency axis, contribute to decrease the reflection coefficient, which is below −34 dB for all the optimized frequency range.

Table II. Geometrical parameters of the optimized multilayer structure of total thickness $L = 10$ cm.

	$n = 1$	$n = 2$	$n = 3$	$n = 4$
$L_p^{[n]}$ (cm)	3.00	3.00	2.16	1.85
$L_0^{[n]}$ (cm)	0	0	0	0
σ (kRayls/m)	2.35	7.06	20.01	50.00

We can see that, as occurs in the previous case, it lacks of air cavities. Note that the flow resistivity does not reach the bound of the optimization constraints for any layer (1000 Rayls/m). Then, the impedance matching at the lower frequencies can be fulfilled by using only porous layers. In the case of using higher flow resistivity materials, as well as in the case of thicker multi-layered structures, the optimization process results in air layers at the beginning of the structure. This is in according to Section 4: the air layers decrease the intrinsic losses and optimize the impedance matching with the surrounding medium. However, as occurs in the case of $L = 5$, no perfect absorption can be achieved below the first quarter-wavelength resonance because this kind of structures lack of deep-subwavelength resonances.

6. Conclusions

We have shown the conditions to obtain perfect absorption in rigidly-backed layers of high-porous materials. Due to the close characteristic impedance of these materials with the surrounding air and its high intrinsic losses, perfect absorption can be observed by tuning the thickness of the layer and its properties. The absorption performance of several configurations was analyzed.

On the one hand, in the case of a single rigidly-backed layer of high- porous material, and using the DB or the DBM models, the frequency at which the perfect absorption is observed is around the Biot frequency of the high-porous material, which is fixed by the material parameters. The optimal flow resistivity shows an almost linear dependence with the desired quarter-wavelength resonance frequency. Using other models for the high-porous media as the JCA or JCAL nearly similar relations were found, only a different behavior was observed at low frequencies. The optimal thickness of the layer to obtain perfect absorption at its quarter-wavelength resonance was found to be $L \approx \lambda_0/4.3$ for DB model, $L \approx \lambda_0/4.64$ for DBM model, while bigger ratios were observed using JCA and JCAL models, mainly due to tortuosity effects.

On the other hand, the behavior of the perfect absorption for oblique angles of incidence was presented. By tilting the incidence angle the material can be impedance matched at others frequencies using the quarter-wavelength resonance and also its higher harmonics when the layer of material is thinner than the optimal one. How-

ever, for layers much thicker than the optimal one, tilting the incidence angle does not produce perfect absorption.

For the case of a high-porous layer with a rigidly-backed air cavity, we show that the air cavity can provide perfect absorption for structures composed by high flow resistivity porous material, i.e., structures thicker than the optimal layer. This is caused by the decreasing of the total intrinsic losses when the air gap is introduced. In contrast, for structures thinner than the optimal one, introducing an air gap do not produce perfect absorption because the leakage of the structure at the resonance is increased.

In addition, porous multilayer structures were optimized to provide broadband and perfect absorption. We showed that using optimized structures very flat curves of absorption can be obtained due to the progressive impedance matching. This is in accordance with other works that analyzed graded porous materials [24]. However, due to the lack of any deep-subwavelength resonance, the absorption cannot be increased below of the quarter-wavelength resonance of the slab of equivalent material. To obtain perfect absorption in a deep-subwavelength thickness layer the system should present a subwavelength resonance in addition to the impedance matching. This can be accomplished by the use of deep-subwavelength resonators [12, 13] or by the reduction of the sound speed in the slab of equivalent material [8, 10, 11]. In addition, the recent development of 3D printing capabilities can be exploited to manufacture porous materials with a micro-structure that provides specific design parameters (flow resistivity, tortuosity, porosity, ...). Using this approach, one can design porous materials that fulfill the conditions for perfect absorption of sound presented in this work.

Finally, the use of the complex frequency plane to obtain the critical coupling conditions offers a deep physical insight of the system, showing the balance between the intrinsic losses and leakage of the structure due to the resonance, then, helping to understand the system and providing means to design perfect absorbing structures. Thus, by using the frequency complex plane analysis one can determine if the system lack or exceeds the losses, allowing the fine tuning of the system to design perfect sound absorbing structures in a general framework. The parametric analysis in this work has been restricted to high-porous materials showing the tendencies and the main guidelines to obtain perfect absorption by using porous layers. The physical insight shown in this work by the complex frequency plane is general and can be extended to other range of parameters with bigger tortuosity or porosity without any loss of generality.

Acknowledgment

The authors acknowledge financial support from the Metaudible Project No. ANR-13-BS09-0003, co funded by ANR and FRAE. This article is based upon work from COST Action DENORMS CA 15125, supported by COST (European Cooperation in Science and Technology).

References

[1] J. Allard, N. Atalla: Propagation of sound in porous media: modelling sound absorbing materials 2e. John Wiley & Sons, 2009.

[2] T. J. Cox, P. D'Antonio: Acoustic absorbers and diffusers: theory, design and application. 3rd ed. CRC Press, 2016.

[3] N. Jiménez, V. Romero-García, V. Pagneux, J.-P. Groby: Quasiperfect absorption by subwavelength acoustic panels in transmission using accumulation of resonances due to slow sound. Phys. Rev. B **95** (2017) 014205.

[4] V. Romero-García, G. Theocharis, O. Richoux, V. Pagneux: Use of complex frequency plane to design broadband and sub-wavelength absorbers. The Journal of the Acoustical Society of America **139** (2016) 3395–3403.

[5] A. Merkel, G. Theocharis, O. Richoux, V. Romero-García, V. Pagneux: Control of acoustic absorption in one-dimensional scattering by resonant scatterers. Appl. Phys. Lett. **107** (2015) 244102.

[6] M. Yang, C. Meng, C. Fu, Y. Li, Z. Yang, P. Sheng: Subwavelength total acoustic absorption with degenerate resonators. Appl. Phys. Lett. **107** (2015) 104104.

[7] C. Lagarrigue, J. Groby, V. Tournat, O. Dazel, O. Umnova: Absorption of sound by porous layers with embedded periodic arrays of resonant inclusions. J. Acoust. Soc. Am. **134** (2013) 4670–4680.

[8] J.-P. Groby, R. Pommier, Y. Aurégan: Use of slow sound to design perfect and broadband passive sound absorbing materials. J. Acoust. Soc. Am. **139** (2016) 1660–1671.

[9] Y. Li, B. M. Assouar: Acoustic metasurface-based perfect absorber with deep subwavelength thickness. Appl. Phys. Lett. **108** (2016) 063502.

[10] N. Jiménez, W. Huang, V. Romero-García, V. Pagneux, J.-P. Groby: Ultra-thin metamaterial for perfect and quasi-omnidirectional sound absorption. Applied Physics Letters **109** (2016) 121902.

[11] N. Jiménez, V. Romero-García, V. Pagneux, J.-P. Groby: Rainbow-trapping absorbers: Broadband, perfect and asymmetric sound absorption by subwavelength panels for transmission problems. Scientific Reports **7** (10 2017) 13595.

[12] J. Mei, G. Ma, M. Yang, Z. Yang, W. Wen, P. Sheng: Dark acoustic metamaterials as super absorbers for low-frequency sound. Nat. Commun. **3** (2012) 756.

[13] G. Ma, M. Yang, S. Xiao, Z. Yang, P. Sheng: Acoustic metasurface with hybrid resonances. Nat. Mater. **13** (2014) 873–878.

[14] V. Romero-García, G. Theocharis, O. Richoux, A. Merkel, V. Tournat, V. Pagneux: Perfect and broadband acoustic absorption by critically coupled sub-wavelength resonators. Sci. Rep. **6** (2016) 19519.

[15] M. Delany, E. Bazley: Acoustical properties of fibrous absorbent materials. Applied acoustics **3** (1970) 105–116.

[16] Y. Miki: Acoustical properties of porous materials-modifications of delany-bazley models. Journal of the Acoustical Society of Japan (E) **11** (1990) 19–24.

[17] D. L. Johnson, J. Koplik, R. Dashen: Theory of dynamic permeability and tortuosity in fluid-saturated porous media. J. Fluid. Mech. **176** (1987) 379–402.

[18] Y. Champoux, J.-F. Allard: Dynamic tortuosity and bulk modulus in air-saturated porous media. J. Appl. Phys. **70** (1991) 1975–1979.

[19] D. Lafarge, P. Lemarinier, J. F. Allard, V. Tarnow: Dynamic compressibility of air in porous structures at audible fre-

quencies. The Journal of the Acoustical Society of America **102** (1997) 1995–2006.

[20] B. Brouard, D. Lafarge, J.-F. Allard: A general method of modelling sound propagation in layered media. J. Sound Vib. **183** (1995) 129–142.

[21] N. Jiménez, J.-P. Groby, V. Pagneux, V. Romero-García: Iridescent perfect absorption in critically-coupled acoustic metamaterials using the transfer matrix method. Applied Sciences **7** (6 2017) 618.

[22] T. E. Vigran: Building acoustics. CRC Press, 2008.

[23] N. Jiménez, V. Romero-García, A. Cebrecos, R. Picó, V. J. Sánchez-Morcillo, L. M. García-Raffi: Broadband quasi perfect absorption using chirped multi-layer porous materials. AIP Advances **6** (2016) 121605.

[24] S. Mahasaranon, K. V. Horoshenkov, A. Khan, H. Benkreira: The effect of continuous pore stratification on the acoustic absorption in open cell foams. Journal of Applied Physics **111** (2012) 084901.